Can Molten Carbonate be a Non-metal Catalyst for CO Oxidation?

Journal:	*New Journal of Chemistry*
Manuscript ID	NJ-ART-05-2018-002462.R1
Article Type:	Paper
Date Submitted by the Author:	17-Aug-2018
Complete List of Authors:	Tong, Jingjing; University of South carolina, M.E. lei, xueling; Jiangxi normal university, Department of Physics Zhang, Peng; University of South Carolina, Mechanical Engeneering Huang, Kevin; University of South Carolina, Mechanical Engineering Mbamalu, Godwin; Benedict College Qin, Changyong; Benedict College, Biology and Chemistry

New Journal of Chemistry

ARTICLE

Can Molten Carbonate be a Non-metal Catalyst for CO Oxidation?

Jingjing Tong [a], Xueling Lei [a,b], Peng Zhang [c], Kevin Huang [c], Godwin Mbamalu [a] and Changyong Qin [a,]*

Received 00th January 20xx,
Accepted 00th January 20xx

DOI: 10.1039/x0xx00000x

www.rsc.org/

For the first time, we have examined molten carbonate as a non-metal catalyst for the CO oxidation at the temperature of 300~600 °C. The reaction mechanism was analyzed using a classic Langmuir-Hinshelwood model combined with DFT calculations. It was found that the conversion of CO is largely inhanced by molten carbonate at about 400°C and increased to 96% at 500 °C. The reaction process involves four steps, including (1) dissociative adsorption of oxygen, (2) adsorption of CO, (3) surface reaction, and (4) desorption of CO_2. DFT modeling reveals the formation of $(C_2O_4)^{2-}$ and $(CO_4)^{2-}$ as the intermediate species, and that the first two steps are exothermic and preferred by chemical equilibrium. The energy barrier of oxygen dissociation to form CO_4^{2-} is calculated to be 23.0 kcal/mol, which is in a good agreement with the measured overall activation energy of 19.1 kcal/mol. However, the surface reaction (step 3) has a low energy barrier of 10.8 kcal/mol only. This confirms that the oxygen dissociation is the rate determing step in the whole process. Further analysis of the reaction kinetics indicates that the reaction is affected by the CO concentration. With low CO concentration, the reaction is the first order with respect to CO and half order to O_2. From the current report, it has been proven that molten carbonate can serve as an efficient catalyst for CO oxidation and potentially for other oxidation reactions at the temperature range of 400 ~ 600°C. More studies are demanded to further deliberate the reaction mechanism and explore more potential industrial applications.

1. Introduction

Carbon monoxide (CO) is not only toxic to human and environment but also a poison to many metal catalysts in industrial processes. The easiest way to remove CO is to turn it into carbon dioxide (CO_2), a less toxic and inert gas. Precious metals have been mostly promoted for such a purpose with many promising performances observed. For example, Bond et al. have firstly demonstrated Pd/SnO_2 as an excellent CO oxidizing catalyst at the temperature of 120-200 °C [1]. More recently, Stark and Harris developed the catalyst systems of Pd/SnO_2 and Pt/SnO_2 with high conversion efficiency. Those were successfully deployed to CO_2 laser systems [2-3]. Additionally, other metal catalysts such as Au/MnO_2 [4-6], Au/Fe_2O_3 [7-8], Pt/Al_2O_3 [9-11], Ru-Pt [12-13] and Ag/MnO_2 [14-15] have also been extensively investigated for catalyzing the oxidation of CO at ambient or low temperatures. Significant potential applications for such systems include CO_2 laser, auto exhaust gas treatment, gas purification and mine rescue.

To reduce or remove the usage of precious metals as they are of high cost and limited resource availability, many efforts have been geared towards low-cost transition metals and their oxides [16-18]. For example, Wang et al. prepared a copper-based catalyst of 7.5Cu/10SDC and achieved a conversion of 97% at 175 °C [19]. Kang et al. reported a catalyst of CoO_x/CeO_2 with a very low reaction temperature and good water vapor resistance [20]. It was proposed that highly dispersed Co at high valence state plays an important role in the process of CO oxidation. Arena et al. have examined the nanostructured MnCeOx as a catalyst for the reaction of CO oxidation. The effect of cerium concentration on the activity, structure and reducibility of the catalyst was evaluated. Its reaction mechanism and kinetic model were also proposed [21, 22]. More recently, nanostructures like graphene [23-24], nanotube [25-26], zeolite [27], and MOF [28-29] have also been extensively examined for the oxidation of CO. As we know, the gas mixtures are at very high temperatures in certain cases such as combustion engine exhaust and industry processes, which may cause dramatic change of the geometrical and electronic structure, and chemical reactivity for the metal-based catalysts. Finally, the catalysts will be degraded. Therefore, catalytic systems for CO oxidation at intermediate temperatures are needed.

In the past decades, molten carbonates (MC) have been used in the fuel cells as electrolyte [30-31] and CO_2 separation membrane [32-33]. Recently, they were introduced into the cathode of solid oxide fuel cells (SOFC) as a booster for the reaction of oxygen reduction.

[a] *Department of Biology, Chemistry and Environmental Health Science, Benedict College, Columbia, South Carolina 29204, USA*
[b] *Department of Physics, Jiangxi Normal University, Nanchang, Jiangxi 330022, China*
[c] *Department of Mechanical Engineering, University of South Carolina, Columbia, South Carolina 29207, USA*
* Corresponding author: Changyong Qin, Changyong.Qin@benedict.edu

Qin et al. studied the dissociative adsorption of oxygen in MC using density functional theory (DFT) modeling and found that oxygen exists in MC as perocarbonate (CO_4^{2-}) [34]. In CO_4^{2-}, an oxygen atom is carried by a carbonate ion and considered as a strong oxidizing agent. To prove the concept that MC could be a possible non-metal catalyst for oxidization, we have performed a combined experimental and computational study of CO oxidation catalyzed by MC in the current report. To our knowledge, this is the first time to use liquid phase molten salt to catalyze the CO oxidation and will open a door for developing non-metal eco-friendly catalysts for different industrial and environmental processes in the future.

2. Experimental and Computational Methods

2.1 Catalyst preparation

Ternary eutectic molten carbonate of Li/Na/K was adopted in the research due to its low melting point of about 398°C. Molten carbonate was deposited on the surface of commercial Al_2O_3 pellets (1/8" pellets, high surface area, Alfa Aesar) and used as CO oxidation catalyst. Li_2CO_3 (Alfa Aesar, 99.8%), Na_2CO_3 (Alfa Aesar, 99.9%) and K_2CO_3 (Alfa Aesar, 99.8%), the precursors of the ternary molten carbonate, were dissolved in deionized water in a molar ratio of 42.5 : 32.5 : 25.0 (the composition of lowest eutectic point of Li/Na/K ternary molten carbonate) to form a saturated aqueous solution. The catalyst (MC/Al_2O_3) was prepared by impregnation of porous Al_2O_3 with the ternary carbonate aqueous solution. More specifically, the Al_2O_3 porous pellets were soaked in carbonate solution for approximately 4 hours in a vacuum chamber (10kPa), then dried in an oven at 80 °C for 12 hours and followed with calcination at 120 °C to remove the moisture. The MC load was approximately 1.0% by weight.

2.2 Catalyst characterization

The microstructure and the composition of the catalyst before and after testing were analyzed by scanning electron microscopy (SEM, Zeiss FESEM) combined with an energy dispersive X-ray spectroscopy (EDS). The catalytic oxidation of carbon monoxide was carried out in a horizontal flow reactor, illustrated in Fig. 1. The catalyst, 20g MC/Al_2O_3 (approximately 0.2g MC), was loaded to the center of the alumina tube and packed tightly with two porous ceramic pellets. A mixture of CO and air was fed in from one side of the reactor and collected from the other side. The flow rate of each gas was controlled by a mass flow controller (Alicat Scientific, MC-50SCCM-D/5M), while soak film flow meter was used for calibrations. The flow rate of CO was controlled at 6.76 sccm, while the total flow maintained at 100 sccm. The actual total flow rate of inlet gas (feed gas) and outlet gas (product gas) was measured by the soak film flow meter and used for calculating the CO conversion. The outlet gas was analyzed by a CO_2 detector (Vernier, CO_2 sensor) to identify the concentration of the CO_2. The concentration of CO_2 was tested every 10 °C from 300~600 °C. At

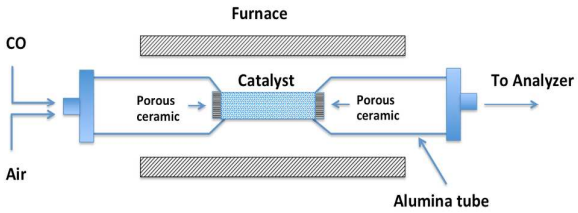

Fig. 1 Illustration of the tubular reactor for the catalyst testing

each temperature point, the system was held at least for 30 min before measuring the CO_2 concentration. The CO_2 content is then used to evaluate the CO conversion as a function of temperature.

For the reaction of CO oxidation, CO + ½ O_2 → CO_2, the amount of CO consumed should equal to that of CO_2 produced. Therefore, the CO conversion as percentage can be calculated by:

Conversion $= F'_{CO2}/F_{co} = (F'_{total} \times C_{CO2})/F_{CO}$,

where F'_{total} is outlet gas total flow rate, F'_{CO2} is CO_2 yield flow rate in outlet gas, C_{CO2} is the concentration of CO_2 in the outlet gas, and F_{CO} is the CO feed flow rate.

2.3 DFT Modeling

All structures were optimized at the B3LYP [35-36]/6-31G(d,p) [37-40] level using the Gaussian 09 program[41]. All stationary points on the potential energy surface (PES) were then verified by calculated vibrational frequencies at the same theoretical level. Therefore, the reactant and product structures are truly local minima while each transition state is at the first order saddle point. The reaction pathway, i.e. the connection between reactant, TS and product, was verified by the intrinsic reaction coordinate (IRC) calculations. In addition, the zero-point energy (ZPE) correction was performed for all calculated energies.

3.Results and discussion

3.1Physical characterization

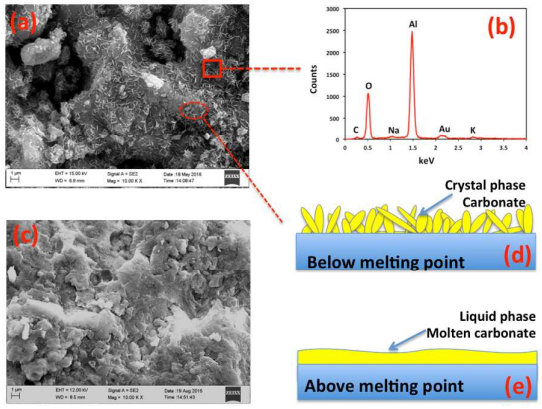

Fig. 2 SEM images of (a) molten carbonate (MC) on Al_2O_3 support; (b) EDS result of MC on the Al_2O_3; (c) Al_2O_3 pellet support; (d) schematic of solid phase of MC on the Al_2O_3; (e) schematic of MC on the Al_2O_3 above melting point

Fig. 2(a) shows the SEM images of the MC/Al_2O_3 catalyst before test at room temperature. The flake like crystal is the MC phase, which covers almost all the surface of the Al_2O_3 support comparing to pure Al_2O_3, as shown in Fig. 2(c). To further confirm the composition of the crystal phase, EDS was involved to test the composition of the red square area in Fig. 2(a), and the result was shown in Fig. 2(b). Na, K, C and O were observed in the EDS spectrum, indicating that the crystal phase is the molten carbonate. Li didn't show up in the spectrum because it is too light to be detected by EDS. Element Al is from the Al_2O_3 support, and Au is from the Au coating, which had to be added for the SEM imagining. A schematic of the MC/Al_2O_3 catalyst below melting point is shown in Fig. 2 (d), while Fig. 2 (e) for its structure above the melting point.

3.2 Catalytic reaction evaluation

Fig. 3 shows the conversion of the carbon monoxide to carbon dioxide with and without the presence of the MC/Al_2O_3 catalyst. It is found that the CO conversion with MC/Al_2O_3 is higher in the whole temperature range of 300~600 °C, showing a good catalytic performance of MC/Al_2O_3 for the oxidation of CO. Two inflection points are shown in the conversion curve of MC/Al_2O_3. The first inflection point is at about 400°C, which is the melting point of the MC. Below 400 °C, the CO conversion on solid phase MC is very low, but still much higher

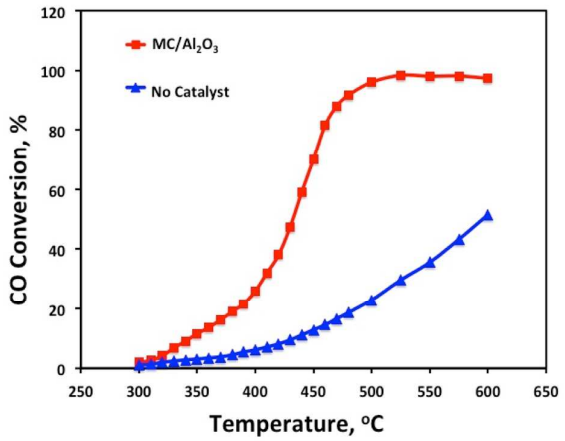

Fig. 3 CO conversion *vs.* Temperature.

than that with no MC catalyst. However, the CO conversion on liquid melt phase increases dramatically with the temperature increase from 400 °C to 500 °C. The CO conversion by MC/Al_2O_3 reaches 96% at 500°C, while only 25% at the same temperature without the catalyst. The results indicate that both solid phase and liquid phase MCs present some catalytic activity for the CO oxidation, but the liquid phase has a much higher catalytic activity. The second inflection point is at 500°C, the conversion curve becomes flat and stabilized at 96-98% due to the fact that most of CO has been converted to CO_2

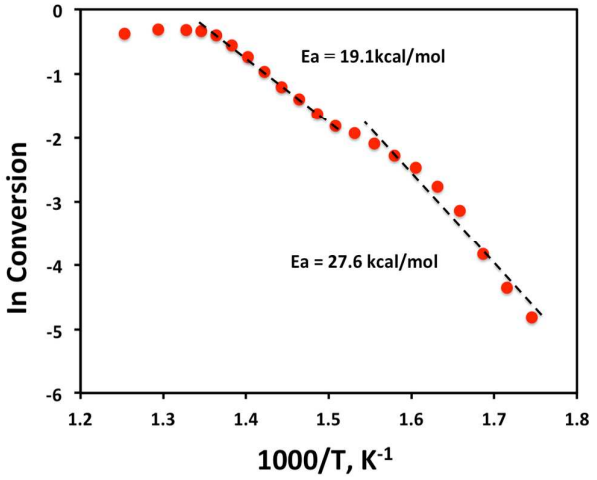

Fig. 4 Arrhenius plot of calibrated CO conversion

Fig. 4 shows the Arrhenius plot of CO conversion by MC/Al_2O_3 as a function of 1000/T (K^{-1}). Since the measured CO conversion rate includes contributions from not only the catalytic reaction but also the gas phase reaction itself, the conversion rate for the Arrhenius plot was corrected by deducting the CO conversion rate without catalyst. Below the melting temperature (300-390°C), the activation energy (Ea) is found approximately to be 27.6kcal/mol. While above the melting point (390-480°C), the Ea value is decreased to 19.1kcal/mol. Such a large difference in Ea implies that the reaction may proceed through different pathways on the solid and melted MC. A very good linear relationship between ln(conversion) and 1000/T (r^2=0.99) was observed, showing the CO oxidation on MC a first order reaction. Above 500 °C, the gas phase reaction of CO and oxygen is significant and it becomes extremely difficult to evaluate the contribution from the catalyst itself. So we did not calculate the activity energy beyond 500 °C.

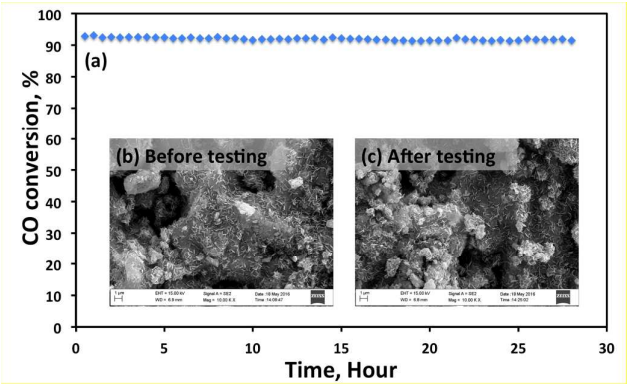

Fig. 5 (a) CO conversion as a function of time; (b) SEM image of MC/ Al_2O_3 catalyst before test; (c) SEM image of MC/ Al_2O_3 catalyst after test.

Fig 5 (a) shows the CO conversion over MC/Al_2O_3 catalyst at 480°C with a feed gas of 6.67% CO air balance within 28 hours. The conversion rate remained very stable at ~98% during this 28-hour stability test. The weight of catalyst was measured to be same before and after the test, indicating no loss of the MC catalyst during the reaction process. In addition, no change was observed for the microstructure of the catalyst before (Fig. 5(b)) and after the test (Fig. 5 (c)). Such evidences imply

that molten carbonate is stable for the reaction of CO oxidation at 300-500°C. This finding agrees well with the results by many others on the research of molten carbonate fuel cells (MCFC) where MC was used as electrode at >500 °C. [30-31]

3.3 Reaction mechanism

Assuming that the reaction will proceed through a Langmuir-Hinshelwood (L-H) mechanism, which can be described by Eqn. (1-3). Using DFT methods, those three steps have been investigated to help understand the reaction kinetics and mechanism. The enthalpy change is calculated to be -0.3 kcal/mol and -36.4 kcal/mol at the B3LYP/6-31G(d) level for Eqn. (1) and (2), respectively. This indicates that both oxygen dissociation and CO adsorption are exothermic and favored by chemical equilibrium, but the step of Eqn. (2) is much more favored, i.e. $K_2 >> K_1$. However, the step of Eqn. (1) has an energy barrier of about 23.0 kcal/mol calculated by DFT in pure lithium carbonate [34].

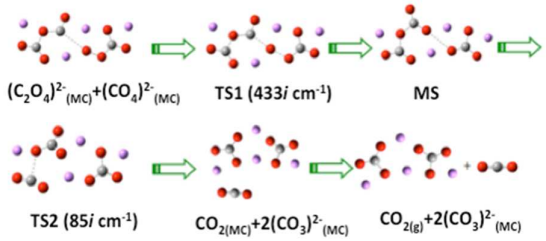

Fig. 6 Structural evolution of the reaction process calculated by DFT

$$\frac{1}{2}O_{2(g)} + (CO_3)^{2-}_{(MC)} \overset{K1}{\leftrightarrow} (CO_4)^{2-}_{MC} \quad (1)$$

$$CO_{(g)} + (CO_3)^{2-}_{(MC)} \overset{K2}{\leftrightarrow} (C_2O_4)^{2-}_{MC} \quad (2)$$

$$(C_2O_4)^{2-}_{MC} + (CO_4)^{2-}_{(MC)} \rightarrow 2(CO_3)^{2-}_{MC} + CO_{2(g)} \quad (3)$$

For the surface reaction of Eqn. (3), DFT calculations were performed using a small cluster of $Li_2(C_2O_4)$-$Li_2(CO_4)$ as shown in Fig. 6. The overall reaction path and potential energy surface (PES) with ZPE corrections are plotted in Fig. 7. At the initial state, both CO and O_2 are brought to the surface of carbonate catalyst as the molecular form of $(C_2O_4)^{2-}$ and $(CO_4)^{2-}$ and the oxygen and CO are pointing to each other, highlighted by red and blue circles, respectively. Once the oxygen atom leaves its carbonate carrier, it will approach CO of $(C_2O_4)^{2-}$ and this leads to a transition state (TS1). At TS1, the O-O bond is breaking, while the C-O bond is forming as highlighted in the orange circle. Next, CO_2 is formed, but it is attached to a carbonate ion, forming an intermediate state of pyrocarbonate $(C_2O_5)^{2-}$. The same structure was identified by Huang et al. and reported in Ref. [42]. Through another transition state (TS2), CO_2 is released and finally detached from the surface of MC. From Fig. 7, the energy barrier for the surface reaction of Eqn. (3) is calculated to be only 10.8 kcal/mol.

From classical Langmuir-Hinshelwood mechanism, the reaction rate can be described by:

$$r = kC^2_{CO_3^{2-}} \frac{K_1 K_2 C_{O_2}^{1/2} C_{CO}}{(1+K_1 C_{O_2}^{1/2} + K_2 C_{CO})^2} \quad (4)$$

where r is the reaction rate, k for the rate constant of Eqn. (3), K_1 and K_2 for the equilibrium constant of Eqn. (1) and (2). In terms of CO_3^{2-}, the reaction is of second order, implying an important role the carbonate catalyst plays in the reaction. The reaction is From the DFT results, we can conclude $K_1 C_{O_2}^{1/2} \ll K_2 C_{CO}$, then the reaction rate will be approximated as:

$$r = kC^2_{CO_3^{2-}} \frac{K_1 K_2 C_{O_2}^{1/2} C_{CO}}{(1+K_2 C_{CO})^2} \quad (5)$$

If the concentration of CO is extremely low, then $K_2 C_{CO} \ll 1$ and the reaction rate is approximated as

$$r = kK_1 K_2 C_{O_2}^{1/2} C_{CO} C^2_{CO_3^{2-}} \quad (6)$$

The reaction is the first order with respect to CO, while half order for O_2. Increase of the concentration of reactant, both CO and O_2, will increase the reaction rate. On the other hand, if the CO concentration is very high, then $K_2 C_{CO} \gg 1$ and the reaction rate is described by the equation of

$$r = kC^2_{CO_3^{2-}} \frac{K_1 C_{O_2}^{1/2}}{K_2 C_{CO}} \quad (7)$$

In this case, the CO molecules will cover the catalyst surface and will inhibit the reaction. This should make the reactor more difficult and experience higher overall energy barrier. In the current experiment setting, the effect of the concentration of CO was not investigated yet and will be reported in the future.

In Fig. 7, the reaction path is described by the PES as a function

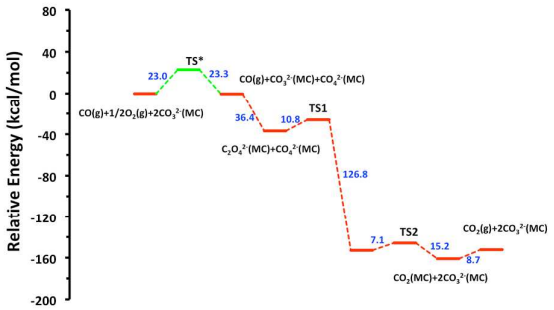

Fig. 7 Reaction path and potential energy surface

of reaction coordinate. The green part of oxygen dissociation in molten carbonate is from Ref. [34]. The reaction is initiated by oxygen dissociation, and then undergoes with CO adsorption, surface reaction of absorbed species, and finally desorption of CO_2. The rate-determining step is oxygen dissociative adsorption with an energy barrier of 23.0 kcal/mol, while the surface reaction is relatively easy with calculated activation energy of 10.8 kcal/mol. The actual activation energy through Arrhenius plot method (Fig. 4) is measured to be 19.1 kcal/mol. This agrees with the DFT

results. It should be pointed out that the contribution of entropy was not considered in the DFT calculations, but it should have some contributions to the reaction kinetics in such a high temperature reaction system.

Conclusions

In the current study, we have demonstrated molten carbonate as a non-metal catalyst for the CO oxidation at the temperature of 300~600 ^{o}C for the first time. The conversion is largely enhanced by melting at about 400^{o}C and increased to 96% at 500 ^{o}C. The reaction mechanism is described by a Langmuir-Hinshelwood model, including four steps: (1) dissociation adsorption of oxygen, (2) adsorption of CO, (3) surface reaction, and (4) desorption of CO_2. DFT modeling reveals the formation of $(C_2O_4)^{2-}$ and $(CO_4)^{2-}$ as the intermediate species. It also shows that the first two steps are exothermic and preferred by chemical equilibrium, but the oxygen dissociation has higher energy barrier than the surface reaction itself and become the rate-determining step in the whole process. The calculated energy barrier for oxygen dissociation to form CO_4^{2-} is 23.0 kcal/mol from Ref. [34], which is in a fairly good agreement with the measured overall activation energy of 19.1 kcal/mol. Further analysis of the reaction kinetics indicates that the reaction is affected by the CO concentration. With low CO concentration, the reaction is the first order with respect to CO and half order to O_2. From this study, it has been proven that molten carbonate can serve as an efficient catalyst for CO oxidation and potentially for other oxidation reactions at the temperature range of 400~600 ^{o}C. More studies are demanded to further deliberate the reaction mechanism and explore more potential industrial applications of such a novel catalyst system.

Acknowledgements

Financial supports of the present work from the Army Research Office (ARO) of the Department of Defense (DoD) (Grant Number: 62940CHREP, 70518CHREP) and the Department of Energy Minority Serving Institution Partnership Program (MSIPP) managed by the Savannah River National Laboratory (SRNL) (SRNS contract number: 0000272359) are greatly appreciated. C.Q. and K.H. would also like to thank National Science Foundation (Grant number: CBET-1264706) for partial support.

References

1 G.C. Bond, L.R. Molloy and M.J. Fuller, *J. C. S. Chem. Comm*., 1975, **829,** 796-797.
2 D.S. Stark and M.R. Harris, *J. Phys. E: Sci. Instrum*, 1983, **16**, 492-496.
3 D.S. Stark, A. Crocker and N.A. Lowde, *J. Phys. E: Sci. Instrum*, 1983, **16**, 11
4 G.B. Hoflund, S.D. Gardner, D.R. Schryer, B.T. Upchurch and E.J. Kielin, *Applied Catalysis B: Environmental*, 1995, **6**, 117-126.
5 S.D. Gardner, G.B. Hoflund, D.R. Schryer, J. Schryer, B.T. Upchurch and E.J. Klelin, *Langmuir*, 1991, **7**, 2135-2139.
6 L. Chang, N. Sasirekha, Y. Chen and W. Wang, *Ind. Eng. Chem. Res*, 2006, **45**, 4927-4935.
7 A.A. Herzing, C.J. Kiely, A.F. Carley, P. Landon and G.J. Hutchings, *Science*, 2008, **321**, 1331-1335.
8 S.T. Daniells, M. Makkee and J.A. Moulijin, *Catalysis Letters*, 2005, **39**, 39-47.
9 G. Avgouropoulos, T. Ioannides, C. Papadopoulou, J. Batista, S. Hovevar and H.K. Matralis, *Catal. Today*, 2002, **75**, 157-167.
10 Y.J. Mergler, A. Van Aalst, J. Van Delft and B.E. Nieuwenhuys, *Applied Catalysis B: Environmental*, 1996, **10**, 245-261.
11 K. Yoshimi, M. Song and M. Ito, *Surface Science*, 1996, **368**, 389-395.
12 S.H. Joo, J.Y. Park, J.R. Renzas, D.R. Butcher, W. Huang and G.A. Somorjai, *Nano Lett*.,2010, **10**, 2709-2713.
13 S. Alayoglu, A.U. Nilekar, M. Mavrikakis and B. Eichhorn, *Nature Materials*, 2008, **7**, 333-338.
14 T. Kou, D. Li, C. Zhang, Z. Zhang and H. Yang, *J. Molecular Catalysis A: Chemical*, 2014, **382**, 55-63.
15 R. Xu, X. Wang, D. Wang, K. Zhou and Y. Li, *J. Catalysis*, 2006, **237**, 429-430.
16 B. Skarman, D. Grandjean, R.E. Benfield and A. Hinz, *J. Catalysis*, 2002, **211**, 119-133.
17 J. Luo, M. Meng, X. Li, Y. Zha, T. Hu, Y. Xie and J. Zhang, *J. Catalysis*, 2008, **254**, 310-324.
18 W. Liu and M.F. Stephanopoulos, *J. Catalysis*, 1995, **153**, 304-316.
19 J.B. Wang, D. Tsai and T. Huang, *J. Catalysis*, 2002, **208**, 370-380.
20 M. Kang, M.W. Song and C.H. Lee, *Applied Catalysis A: Genera*l, 2003, **251**, 143-156.
21 F. Arena, R. Chio, B. Fazio, C. Espro, L. Spiccia, A. Palella, L. Spadaro, *Applied catalysis B: Environmental*, 2017, **210**, 14-22.
22 F. Arena, R. Chio, L. Filiciotto, G. Trunfio, C. Espro, A. Palella, A. Patti, L. Spadaro, *Applied Catalysis B: Environmental*, 2017, **218**, 803-809.
23 Y. Li, Z. Zhou, G. Yu, W. Chen and Z. Chen, *J. Phys. Chem. C.*, 2010, **114**, 6250-6254.
24 Y. Li, Y. Yu, J. Wang, J. Song, Q. Li, M. Dong and C. Liu, *Applied catalysis B: Environmental*, 2012, **125**, 189-196.
25 W. An, Y. Pei and X.C. Zeng, *Nano. Lett*, 2008, **8**, 195-202.
26 I. Lin, Y. Lu and H. *Chen, Phys. Chem. Chem. Phys.,* 2016, **18**, 12093-12100.
27 N. Miriam, M. Izaskun and B. Angel, *Catalysis Science Technology*, 2016, 6, 2623-2632.
28 H. Noei, O. Kozachuk, S. Amirjalayer, S. Bureekaew, M. Kauer, R. Schmid, B. Marler, M. Muhler, R. A. Fischer and Y. Wang, *J. Phys. Chem. C*, 2013, **117**, 5668-5666.
29 J. Ye, C and Liu, *Chem. Commun*., 2011, **47**, 2167-2169.
30 J. Huijsmans, G. Kraaij, R. Makkus, G. Rietveld, E. Sitters, H. Reijers, J. Power Sources, 2000, **86**, 117-121.
31 F. Yoshiba, H. Morita, M. Yoshikawa, Y. Mugikura, Y. lzaki, T. Watanable, M. Komoda, Y. Masuda, N. Zaima, J. Power Source, 2004, **128**, 152-164.
32 L. Zhang, N. Xu, X. Li, S. Wang, K. Huang, W. harris, W. Chiu, Energy Environ. Sci, 2012, **5**, 8310-8317.
33 J. Tong, X. Lei, J. Fang, M. Han, K. Huang, J. Mater. Chem. A, 2016, **4**, 1828-1837.
34 X. Lei, K. Haines, K. Huang and C. Qin, *J. Phys. Chem. A* , 2015, **119**, 8806-8812.
35 C. Lee, W. Yang and R.G. *Parr, Phys. Rev. B*, 1988, **37**, 785.

36 A.D. Becke, *J. Chem. Phys.*, 1933, **98**, 5648.
37 M.M. Francl, W.J. Pietro, W.J. Hehre, *J. Chem. Phys*., 1982, **77**, 3654.
38 J. Blaudeau, M.P. McGrath, L.A. Curtiss and L. Radom, *J. Chem. Phys.*, 1997, **107**, 5016.
39 V.A. Rassolov, J.A. Pople, M.A. Ratner and T.L. Windus, J. Chem. Phys., 1988, **109**, 1223.
40 V.A. Rassolov, M.A. Ratner, J.A. Pople, P.C. Redfern and L.A. Curtiss, *J. Comp. Chem*., 2001, **22**, 976.
41 M.J. Frisch, et al. Gaussian 09, Revision B. 01, Gaussian Inc., Wallingford CT, 2010.
42 L. Zhang, X. Huang, C. Qin, K. Brinkman, Y. Gong, S. Wang and K. Huang, *Phys. Chem. Chem. Phys.*, 2013, **15**, 13147-13152.